

## Generation of coherent undulator radiation using a relativistic photoelectron beam with picosecond micropulses

Young Uk Jeong, Chang Hee Nam, and Sang Soo Lee

*Department of Physics, Korea Advanced Institute of Science and Technology, 373-1, Kusung-dong, Yusung-ku, Taejon, Korea*

Yoshiyuki Kawamura and Koichi Toyoda

*Riken, The Institute of Physical and Chemical Research, Wako-shi, Saitama 351-01, Japan*

(Received 9 April 1992; revised manuscript received 25 August 1992)

The coherent effect of undulator radiation is investigated using relativistic photoelectron beam (RPE) produced by the fourth harmonics of a  $Q$ -switched Nd-doped yttrium aluminum garnet (Nd-YAG) laser. The  $Q$ -switched laser pulse contains a burst of 30 ps micropulses superposed with a weak 8 ns pulse. The current and shape of the RPE were controlled by changing the incident laser intensity. The temporal structure of the RPE was measured using the Cherenkov radiation emitted by relativistic electrons impinging on an optical fiber. When the irradiated laser intensity is stronger than  $5 \text{ MW/cm}^2$ , the wave form of the RPE does not show any microstructure, which is due to the saturation of the RPE current density by space-charge effect. The measured radiation power from the RPE having no microstructure was near the noise level of a microwave diode, even though the current was much larger than that of the RPE having micropulses. With irradiated intensity less than  $1 \text{ MW/cm}^2$ , the temporal structure of the RPE closely follows that of the laser pulse. The measured power of the undulator radiation generated by micropulses was more than  $10^3$  times stronger than that of the theoretically predicted incoherent radiation and tends towards a quadratic dependence on the electron-beam current. The enhancement and tendency is due to coherent radiation emitted by electron-beam micropulses whose typical bunch lengths are comparable to the radiation wavelength (7.4 mm).

PACS number(s): 41.60.Cr, 42.72.-g

### I. INTRODUCTION

An undulator is a periodic electromagnetic structure designed to produce quasimonochromatic synchrotron radiation from relativistic particles [1–15]. Usually such an undulator consists of a set of static magnets. The spectrum of the emitted radiation from wiggling particles depends on the speed of the electron. Electrons moving in a sinusoidal orbit radiate electromagnetic waves of wavelength peaked at

$$\lambda \sim \lambda_w / 2\gamma^2,$$

where  $\lambda_w$  is the wavelength of the undulator periods and  $\gamma = 1/(1-\beta^2)^{1/2}$ . The entire spectrum of radiation starting from microwaves and extending to x rays can be obtained from electrons with energies ranging from 1 MeV to 1 GeV.

The analysis of the radiation emitted by wiggling particles was first discussed by Motz [1] using standard methods of classical electrodynamics. Theoretical [1–12] and experimental [13–15] investigations of this radiation have been carried out by several authors. In the case of normal undulator radiation, referred to hereafter as incoherent undulator radiation, the radiation power scales as  $N$ , where  $N$  is the number of electrons in a bunch. This is caused by the fact that the cross term of the electric field emitted by each electron sums zero by the randomness of the radiation phase. If the phase difference of the radiation could be within constructive range, the ra-

diation power will scale as  $N^2$ , which can significantly enhance the radiation power.

Recently the coherent effects of synchrotron radiation by a bending magnet [17] and of Cherenkov radiation [18] have been observed in a wavelength region comparable to the longitudinal electron bunch length. We have developed a laser-irradiated photocathode for the study of a millimeter wavelength range free-electron laser (FEL). The typical pulse width of the micropulse in the relativistic photoelectron beam (RPE) is approximately 30 ps following the temporal characteristics of the laser pulse, and the corresponding bunch length of micropulses in the RPE is comparable to the wavelength of the radiation ( $\sim 10 \text{ mm}$ ). Hence an observation of the coherent effect in undulator radiation was successfully carried out [19].

As the power of the coherent undulator radiation is closely related to the pulse width of the electron beam, the measurement system having resolution of several picoseconds for the temporal wave form of the electron beam is necessary. The electron-beam pulse of about 30-ps pulse width was measured by using the Cherenkov radiation emitted by electrons passing through the optical fiber. This simple method, which is discussed in detail in Sec. IV, provides the evidence of the coherent undulator radiation and makes it possible to analyze the radiation. In this paper, by generating and measuring the different temporal structure of electron beams, the coherent effect in undulator radiation is investigated and the power spectrum of the coherent radiation is briefly discussed and compared with the incoherent radiation.

## II. CALCULATION OF THE UNDULATOR RADIATION POWER

The total power  $P_t$  radiated by  $N$  electrons passing through the undulator can be obtained [16,19] and expressed to be

$$P_t = P \left| \sum_j e^{-i\varphi_j} \right|^2 \sim NP + N^2PF, \quad (1)$$

where  $\varphi_j$  is the phase of the radiation emitted by the  $j$ th electron. If we assume sinusoidal motion of electrons in an undulator, the radiation phase difference emitted by two electrons is  $(k - k_w)z$  relative to the observer, where  $k$  and  $k_w$  are the wave number of the radiation and undulator magnetic field, respectively, and  $z$  is the distance between electrons. If electrons are distributed according to a Gaussian distribution, the form factor  $F(\alpha)$  is calculated to be

$$F(\alpha) = \exp[-(k'\alpha/2)^2] \quad (2)$$

for a fixed wavelength of radiation, where  $\alpha$  is the half-width at  $e^{-2}$  of the electron-beam peak value and  $k' = k - k_w$ . In the case of a Gaussian distribution, the full width at half maximum (FWHM) is approximately 1.18 times  $\alpha$  for the same pulse. The form factor varies from 0 to 1, depending on the bunch length of the electron beam. When the bunch length of the electron beam is much longer than the wavelength of the radiation, the value of the form factor decreases to 0 and the coherent effect is negligible in the radiation power. When the pulse width of the electron beam is equal to or shorter than the wavelength of the radiation, the value of the form factor becomes close to 1 and the enhancement of the radiation power with respect to the incoherent radiation power is equal to the number of electrons in the bunch,  $N$ . The total radiation power shown in Eq. (1) can be changed to

$$P_t \sim \begin{cases} NP, & l_p \gg \lambda \text{ (incoherent radiation)} \\ N^2PF, & l_p \leq \lambda \text{ (coherent radiation)} \end{cases} \quad (3)$$

where  $l_p$  is the bunch length of the electron beam and  $\lambda$  is the radiation wavelength. The total calculated radiation power emitted by  $10^{10}$  electrons as a function of the pulse width of the electron beam is shown in Fig. 1 for a Gaussian-type electron distribution and wavelength of 7.4 mm. The radiation power emitted by an electron is assumed to be 1 for simplicity.

The central frequency  $f_0$  of the radiation emitted by an electron is obtained from the undulator dispersion relation and the waveguide dispersion relation of the radiation:

$$2\pi f_0 = \beta_{\parallel} c (k_w + k) \text{ and } (2\pi f_0)^2 = (ck)^2 + (2\pi f_c)^2, \quad (5)$$

where  $\beta_{\parallel}$ , the parallel velocity of the electron divided by the light velocity  $c$ , is determined by the single-particle equation of motion and the equation for energy conservation, and  $f_c$  is the cutoff frequency of the waveguide mode. For the present experimental condition, only the

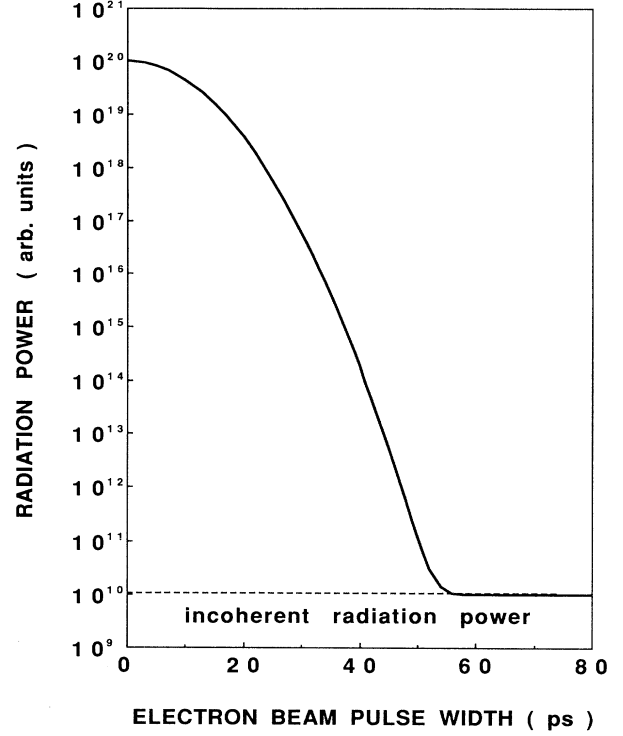


FIG. 1. The theoretically calculated radiation power emitted by  $10^{10}$  electrons as a function of the electron-beam pulse width for a Gaussian-type distribution of electrons and wavelength of 7.4 mm. The radiation power emitted by an electron is assumed to be 1 for simplicity.

TE<sub>10</sub> mode can be excited in an X-band waveguide and the corresponding cutoff frequency is calculated to be 6.55 GHz.

The radiation energy emitted by an electron can be obtained by integrating the spectral energy distribution. The spectral distribution of the energy due to an electron passing through the combined axial guiding magnetic field and the linearly polarized undulator magnetic field in a perfectly conducting rectangular waveguide was studied in Ref. [15]. The spectral distribution of the energy for TE<sub>10</sub> mode is, in cgs units,

$$\frac{dW}{df} \sim C(1 - R^2)^{-2} (\sin\tau/\tau)^2, \quad (6)$$

$$\tau = N_w \pi (f_0 - f) / f_0, \quad (7)$$

$$C = \pi^3 e^2 N_w^2 K^2 k k_x^4 / 2\beta_{\parallel} c \gamma^2 k_g k_c^2 k_w^2 ab,$$

where  $K = eB_w / k_w mc^2$ ,  $R = eB_g / k_w \beta_{\parallel} \gamma mc^2$ ,  $\beta_{\parallel}^* = \beta_{\parallel} c / V_{ph}$ ,  $k_x = \pi/a$ ,  $k_c = 2\pi/\lambda_c$ ,  $k_g = (k^2 - k_c^2)^{1/2}$ ,  $\lambda_c$  is the cutoff wavelength,  $N_w$  is the number of undulator periods,  $ab$  is the cross section of the waveguide, and  $V_{ph}$  is the phase velocity. The term  $(1 - R^2)^{-2}$  in Eq. (6) represents the resonance between the wiggling motion and the cyclotron motion. The total radiation power emitted by wiggling particles can be calculated from Eq. (1) and the integrated form of Eq. (6).

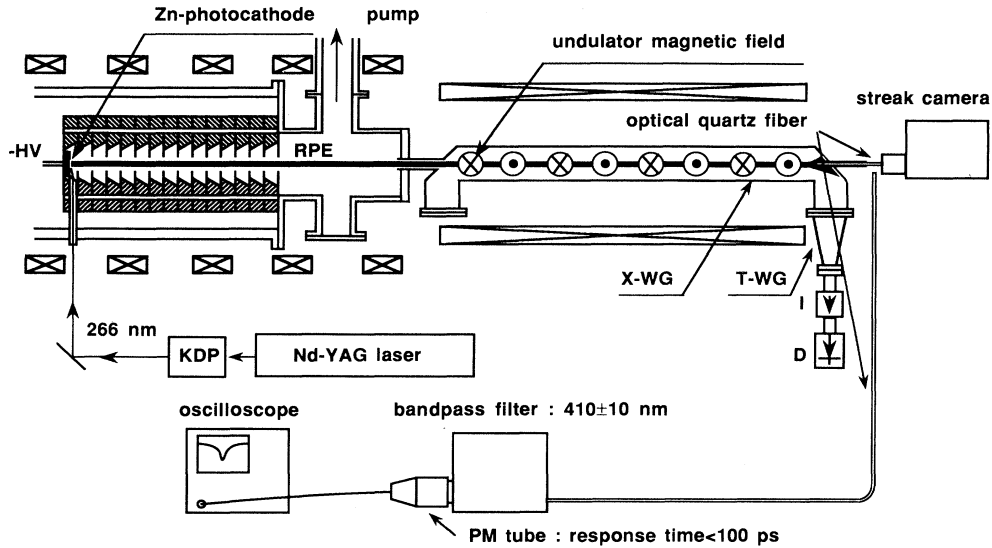


FIG. 2. Schematic diagram of *experimental setup* for measuring spontaneous emission (RPE denotes relativistic photoelectron beam, D denotes 1N26C microwave diode, I denotes isolator, X-WG denotes X-band waveguide, and T-WG denotes tapered waveguide.)

### III. EXPERIMENTAL SETUP

Figure 2 shows the experimental setup for generation and measurement of the undulator radiation. The RPE (610 keV, FWHM = 8 ns) is generated by electrostatically accelerating the photoelectrons produced by the fourth harmonics (266 nm, 15 mJ, 8 ns) of a Q-switched Nd-doped yttrium aluminum garnet (Nd-YAG) laser pulse incident on a Zn cathode. The maximum current and the beam diameter of the RPE in the waveguide are 1.3 A ( $6.6 \text{ A/cm}^2$ ) and 0.5 cm, respectively.

The current-driven undulator magnetic field has a pitch of 5 cm, and the number of undulator periods is 2.5 in the adiabatic region and is 17 in the interaction region. The radiation generated by the RPE is guided by a 120-cm-long X-band waveguide (X-WG,  $2.29 \times 1.02 \text{ cm}^2$ ) and is introduced into a  $K_a$ -band waveguide ( $K_a$ -WG,  $0.71 \times 0.355 \text{ cm}^2$ ) through a tapered waveguide (T-WG). The  $K_a$  band is the IEEE microwave band for the (27–40)-GHz range.

A calibrated microwave diode type 1N26C was used to monitor the wave form of the undulator radiation and measure the radiation power. The microwave diode was calibrated using a reference power of 0.1–30 mW, which was obtained using a calibrated variable attenuator and Gunn oscillator. The rf power of 0.1 mW corresponds to the diode voltage of 1.0 mV. While the microwave diode measured the minimum rf power of  $30 \mu\text{W}$  during the calibration, the sensitivity of the diode in the experiment was limited by the noise signal which was mainly caused by a Marx generator gap switch and high voltage trigger pulse generators (5–70 kV) used to trigger the Marx generator. The noise voltage of the peak to peak in the diode signal was about 0.5 mV, which corresponds to approximately  $50 \mu\text{W}$  power of rf signal. Hence this value of the

noise signal can be neglected within the measurement region of 0.1–30 mW.

The experimental parameters are listed in Table I. Figure 3 shows two central frequencies that can be excited under these experimental conditions according to Eq. (5), which are referred to as upper branch ( $f_u$ ) and lower branch ( $f_l$ ) of the excited central frequencies. The upper branch and lower branch are calculated to be 41.3 and 6.8 GHz, respectively, for this experimental condition. Because the cutoff frequency of the  $K_a$ -band waveguide is 21.1 GHz, the lower branch ( $f_l$ ) was filtered out and could not be introduced into the  $K_a$ -band waveguide. The central wavelength of the radiation is calculated to be 7.4 mm from the value of the upper branch.

TABLE I. Experimental parameters.

TABLE I. Experimental parameters.		
Electron beam	Energy	0.61 MeV
	Current (max.)	1.3 A
	Beam diameter	5 mm
	Pulse width	8 ns (macropulse) 30 ps (micropulse)
Undulator	Type	planar, electromagnet
	Pitch length	5 cm
	Number of periods	2.5 (adiabatic region) 17 (interaction region)
	Magnetic field	0.5 kG
Guiding coil	Magnetic field	2.1 kG
Radiation	Wavelength	7.4 mm

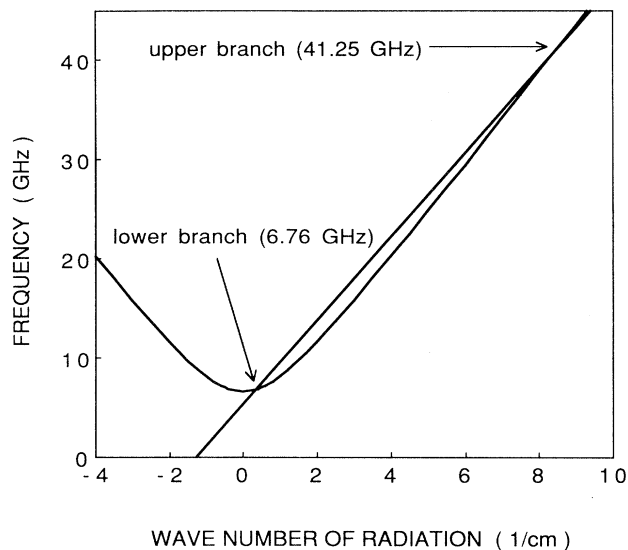


FIG. 3. Two central frequencies obtained by the undulator dispersion relation and the waveguide dispersion relation with the experimental parameters in Table I.

#### IV. MEASUREMENT OF THE TEMPORAL STRUCTURE OF THE RPE

Because the coherent radiation power is closely related to the existence of the RPE microstructure, which will be stated in Sec. V, the measurement of the temporal wave form of the RPE is important in this experiment. The direct measurement of the high-energy electron-beam profile has a number of technical problems, such as high speed disperser of the RPE, the fluorescence plate which would not be damaged by high-energy electrons, and so on. Therefore the temporal wave form of the RPE was changed to a light signal for the optical diagnostic tools [photomultiplier (PM) tube and streak camera] using Cherenkov radiation. The Cherenkov radiation is emitted by the high-energy electron beam passing through an optical quartz fiber. The pulse width measured from the Cherenkov radiation is broader than the actual RPE pulse width due to the dispersion of the multimode quartz fiber and the wide spectrum of the Cherenkov radiation. To know the real wave form, a narrow band pass filter or deconvolution technique must be used.

##### A. Measurement systems for RPE wave form using Cherenkov radiation

Two systems were used for the RPE wave form measurement. First, the entire temporal wave form of the RPE was measured using a 14-m-long optical fiber, optical spectrometer, microchannel plate (MCP) PM tube (spectral sensitivity of 300–650 nm, response time < 100 ps) and 1-GHz oscilloscope (response time  $\sim$  350 ps) in series. The quartz fiber was a multimode fiber with a diameter of 0.3 mm. The optical spectrometer was used to minimize the spectral pulse spreading effect after passing through the long quartz fiber. Cherenkov radiation filtered by the spectrometer had a central wavelength of

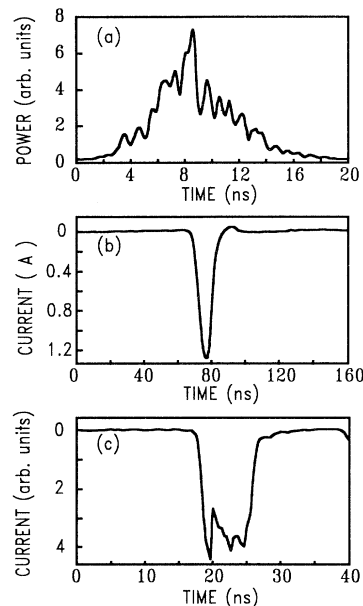


FIG. 4. Oscilloscope photograph of (a) the incident laser wave form measured by a biplanar phototube, (b) the current wave form of the RPE measured using a Faraday cup which is used for the measurement of the total current, and (c) the wave form of the RPE measured using a 14-m-long optical fiber system.

410 nm and the spectral width was 20 nm. The pulse spreading due to the spectral width of 20 nm in the 14-m-long optical fiber is caused by the difference of group velocities in the quartz medium and corresponds to 100 ps. Figure 4 shows the oscilloscope photograph of (a) the temporal shape of incident laser beam measured using a biplanar phototube (response time  $\sim$  100 ps), (b) the wave form of the RPE total current measured using a Faraday cup, and (c) the wave form of the RPE measured from the Cherenkov radiation in the 14-m-long optical fiber.

The microstructure of the RPE was measured using a 43-cm-long optical quartz fiber and a streak camera with a temporal resolution of 8 ps. The intensity of the Cherenkov radiation filtered by the band pass filter was not strong enough for a streak camera measurement. The fiber length of 43 cm was the minimum distance at which the streak camera was not affected by the guiding magnetic field. As we cannot use the narrow band pass filter, the pulse spreading effect in this 43-cm-long optical fiber must be calculated and subtracted. Because the Cherenkov radiation has a wide spectrum from microwave to extreme ultraviolet (XUV), the measured pulse spread due to the difference of group velocities is mainly determined by the sensitivity of the photocathode in the streak camera. The photocathode in the streak camera has spectral sensitivity in the wavelength region from 260 to 660 nm in FWHM. The value of the pulse spreading,  $\Delta\tau$ , by the difference of the refractive index between the wavelength 260 and 660 nm ( $\Delta n = 0.047$ ) is calculated to be approximately 70 ps in a 43-cm-long quartz fiber, which can be easily obtained by using the relation  $\Delta\tau = \Delta n l_f / c$ , where  $l_f$  is the length of the fiber. An addi-

tional pulse spreading effect in the fiber is caused by the path difference of the multimode in fiber. The time delay,  $\Delta\tau_m$ , per unit length of fiber between the light of incident angle 0 and maximum angle that can be transmitted in the fiber is

$$\Delta\tau_m = (NA)^2 / 2nc, \quad (8)$$

where NA is the numerical aperture of the fiber and  $n$  is the refractive index of the fiber. In the case of quartz fiber having a NA of 0.1, this value is calculated to be 5 ps for a 43-cm fiber. Therefore the total value of pulse spread in a 43-cm-long quartz fiber is calculated to be 75 ps and this value is subtracted from the measured value of the electron-beam pulse width.

### B. The temporal structure of the RPE

The current of the RPE could be controlled by changing the power of the fourth harmonics of a Q-switched Nd-YAG laser. Figure 5 shows the current density of the photoelectron as a function of the irradiated laser power density on a Zn photocathode. An optical attenuator for UV light was used to control the RPE current without changing the temporal shape of the irradiated laser beam. When the irradiated laser power density is lower than 3.0 MW/cm<sup>2</sup>, the current density of the photoelectron has a linear dependence on laser power density; this region of the RPE is referred to hereafter as the linear region. The linear dependence of the current density on the laser power density is the result of the single-photon photoelectric effect. When the laser power is more than 5.0 MW/cm<sup>2</sup>, the saturation effect of the photoelectron current density is clearly observed, which is referred to hereafter as the saturated region.

This phenomenon of saturation can be understood

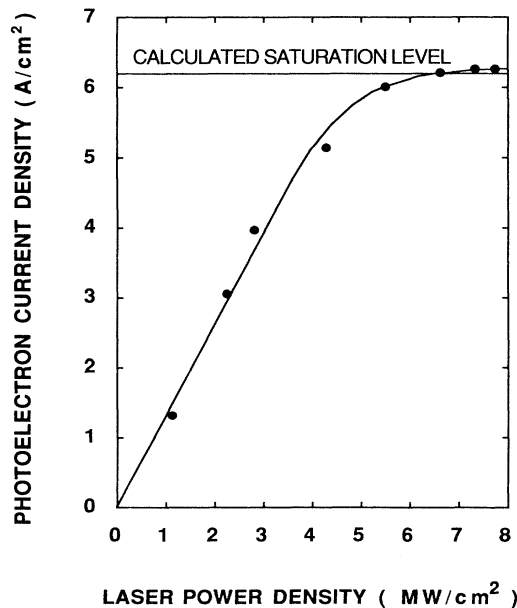


FIG. 5. Measured photoelectron current density with respect to the irradiated laser power density.

from the effect of space-charge limitation of the photoelectron current density. The emitted photoelectrons near the photocathode are accelerated by a planar-type 15-stage gradient ring which equally divides the electric potential. When the density of emitted photoelectrons increases, some photoelectrons return to the cathode due to the negative space charge of high-density photoelectrons, which causes the saturation of photoelectron current density. The emitted photoelectrons change the electric potential between the photocathode and anode, and the space-charge-limited current density can be calculated by considering the modified electric potential between the cathode and the first gradient ring. The space-charge-limited current density for a planar geometry is calculated to be 6.2 A/cm<sup>2</sup> according to the Child-Langmuir law,

$$I = 2.33 \times 10^{-6} V^{3/2} / d^2 \quad (\text{A/cm}^2), \quad (9)$$

where  $V$  is the applied voltage between the cathode and the first gradient ring, and  $d$  is the distance between these two. The calculated saturation level according to Eq. (9) is in good agreement with the experimental result shown in Fig. 5.

A typical wave form of the fourth harmonics of the Q-switched Nd-YAG laser is shown in Fig. 6(a). It was measured using a streak camera with, in this condition, a temporal resolution of 12 ps. The laser pulse contains a burst of micropulses superposed with a weak nanosecond pulse. This is due to the beating of longitudinal modes having 220-MHz spacing and 30-GHz linewidth. The typical FWHM of micropulse was approximately 30 ps. Most of the micropulses are separated by more than 500 ps on the top of the weak 8-ns background pulse.

The temporal wave form of the electron beam was measured using Cherenkov radiation with a streak cam-

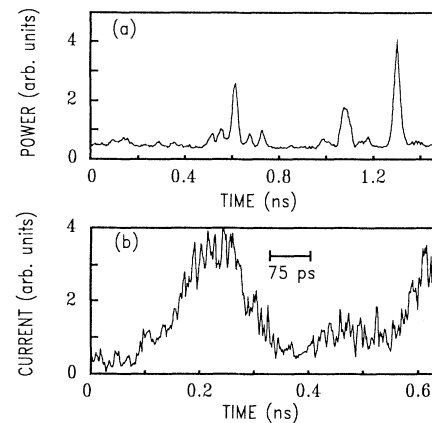


FIG. 6. (a) Typical wave form of the fourth harmonics of a Q-switched Nd-YAG laser pulse which was measured using a streak camera using 12-ps temporal resolution. The typical pulse width of the micropulse is about 30 ps. (b) Typical wave form of the electron-beam micropulse which was measured using the Cherenkov radiation in a quartz fiber and a streak camera. Typical pulse width of the electron-beam micropulse is approximately 35 ps allowing for the pulse spreading effect of 75 ps due to the dispersion of the multimode quartz fiber.

era. The microstructure of the electron current wave form was also observed in the linear region of the RPE. A typical wave form of the electron beam in the linear region is shown in Fig. 6(b). By considering the pulse spreading effect discussed in Sec. IV, the FWHM of a typical micropulse shown in Fig. 6(b) was approximately 35 ps. This value is very close to the typical pulse width of micropulses in the laser pulse. In a nanosecond time scale, it was reported experimentally that the wave form of a photoelectron beam generated from a laser-irradiated photocathode was determined entirely by the temporal shape of incident laser pulse [20,21]. The above result shows that the temporal shape of the photoelectron current follows that of the incident laser pulse within several picoseconds.

The intensity of a micropulse in the incident laser pulse was about five times stronger than that of the weak nanosecond pulse. In the case of the saturated electron beam, the micropulses located temporally in the central part of the electron beam disappeared due to the saturation of the electron-beam current density and the nanosecond pulse component grows with the increase of the laser intensity. When the nanosecond pulse also gets saturated, the flat-top RPE current is obtained in the saturated central part. Figure 7 shows typical wave forms of the saturating electron beams measured by the Cherenkov radiation, which are generated with the incident laser intensity of (a) 1 MW/cm<sup>2</sup>, (b) 3 MW/cm<sup>2</sup>, and (c), (d) 6 MW/cm<sup>2</sup>. The saturation level of the RPE current densi-

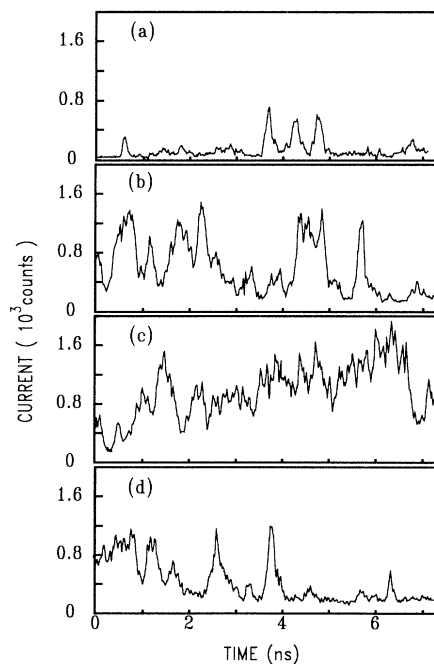


FIG. 7. Typical wave forms of the saturating electron beam, which are generated with the incident laser intensity of (a) 1 MW/cm<sup>2</sup>, (b) 3 MW/cm<sup>2</sup>, and (c), (d) 6 MW/cm<sup>2</sup>. (c) shows the central part of the electron beam, where micropulses are not seen due to the saturation. (d) shows some micropulses surviving in the tail part of the electron beam.

ty is about 1400 counts in the streak camera output, and the nanosecond-long pulse component of the RPE shows the linear dependence on the incident laser intensity. Figure 7(c) shows a section of the electron-beam wave form located temporally in the center, and micropulses are not observed due to the saturation. Figure 7(d) shows a tail part of the electron-beam wave form. There exist unsaturated micropulses because the laser intensity at the leading and trailing edges of the laser pulse is below the saturation level. Both saturated and unsaturated electron beams having different temporal structure were used for comparison in the experiment.

## V. COHERENT UNDULATOR RADIATION

### A. Radiation power enhancement due to the electron-beam microstructure

The spontaneous emission radiated by the saturated electron beam shows a two-peak wave form. Figure 8(a) shows a typical wave form of the radiation by a saturated electron beam of relatively high current ( $\sim 1.25$  A) as shown in Figs. 7(c) and 7(d). The radiation power emitted by the central part of the electron beam having no micropulse was near the noise level of the measurement system. This was in contrast to the result of the radiation power emitted from the head and tail of the electron beam having micropulses, which had a high level of radiation power ( $\sim 0.6$  mW). Figure 8(b) is a typical wave form of the radiation emitted by the unsaturated electron beam with micropulses. Figure 8(b) shows a high level of radiation power ( $\sim 2.5$  mW), even though the total current is 0.43 A, which is much less than that of Fig. 8(a). Micropulses in the central part of the electron beam become smaller and disappear as the incident laser inten-

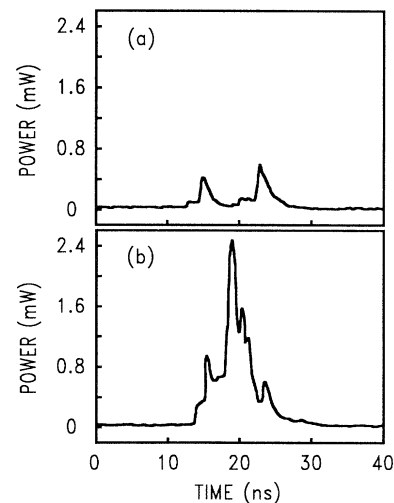


FIG. 8. Typical wave form of the radiation by (a) a saturated electron beam and (b) an unsaturated electron beam. In (a), the radiation power of the central part approaches the noise level in the absence of micropulses. (b) shows the high level of the radiation power, even if the electron-beam current is much less than that of (a). The currents of the electron beam used for (a) and (b) are 1.25 and 0.43 A, respectively.

sity increases from the linear region to the saturated region of the RPE. The radiation power of the central part also decreases to the noise level of the measurement system. The radiation power from both sides of the electron beam reaches the maximum value and becomes smaller during the saturation of the RPE. This anomalous phenomenon is not expected in the case of the incoherent undulator radiation. From these results, one can clearly see the dependence of the radiation power on the existence of micropulses in the electron beam.

The radiation power by the electron beam having micropulses was measured and compared with the theoretically calculated power of the incoherent radiation. Figure 9 shows the measured power of the spontaneous emission as a function of the electron-beam current (solid circles). The dashed line is the theoretically calculated power of the incoherent radiation for an 8-ns RPE current. The number of total electrons is  $3 \times 10^{10}$  for an 8-ns, 0.5-A ( $2.5 \text{ A/cm}^2$ ) RPE current. Each measured value of radiation power is an average of ten shots and the error bar represents the standard deviation of measured power. The measured power of the radiation is more than  $10^3$  times stronger compared to the theoretically calculated power of the incoherent radiation. While the calculated power has a linear dependence on the electron-beam current, the measured power tends towards a quadratic dependence on the RPE current (or the electron number). The enhancement of the radiation power and the quadratic dependence on electron number show the evidence of the coherent effect in the undulator radiation due to the short electron micropulses.

The coherent radiation is affected by the separation distance between micropulses. If we consider the slippage effect which is caused by the velocity difference between the radiation and electrons in an undulator, each electron of the RPE emits radiation of pulse width 500 ps [19]. Therefore micropulses of the RPE emit radiation of pulse width 535 ps. Judging from both the separation of typical micropulses shown in Fig. 6(a) and the number of micropulses which mainly contribute to the radiation power enhancement, the typical separation of micropulses is considered to be more than 500 ps. Because this value of micropulse separation is equal to or larger than that of the slippage distance, an individual micropulse emits radiation independently.

The solid line of Fig. 9 is the fit line of the measured radiation power on the assumption that the measured power is due to coherent radiation. The enhancement ratio between the coherent radiation power  $P_c$  of the fit line and the theoretically calculated power of the incoherent radiation,  $P_{in}$ , is

$$P_c/P_{in} = n_p N_c^2 F(\alpha) / N_{in}, \quad (10)$$

where  $n_p$  is the number of micropulses which contribute to the coherent radiation power,  $N_c$  is the number of electrons in a typical micropulse, and  $N_{in}$  is the number of electrons in a total electron beam. The number of electrons in a micropulse is estimated to be approximately  $5 \times 10^8$  for a 0.5-A RPE current. Judging from the number of peaks contained in the wave form of the undulator radiation, the radiation power is due to the contribution

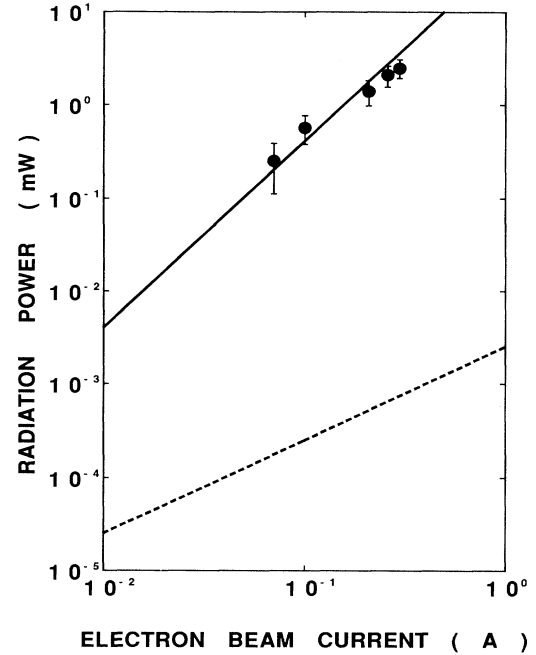


FIG. 9. The measured radiation power (solid circles) of the spontaneous emission as a function of the electron-beam current. Dashed and solid line represent theoretically calculated power of the incoherent and the coherent radiations, respectively. The coherent radiation power is theoretically calculated for radiation with a wavelength of 7.4 mm and an electron-beam pulse width of 33 ps. The number of electrons in a micropulse is estimated to be  $5 \times 10^8$  for a 0.5-A RPE current.

of eight micropulses on average. The enhancement ratio between the coherent radiation power of the fit line and theoretically calculated power of the incoherent radiation is  $7.7 \times 10^3$  for a 0.5-A RPE current. From Eqs. (2) and (10), the pulse width of the electron-beam micropulse corresponding to the fit line is calculated to be 33 ps. For simplicity, the wave form of the electron-beam micropulse is assumed to have a Gaussian distribution. This value of 33-ps pulse width calculated from the fit line which is based on the assumption of coherent radiation is in good agreement with the measured value of the pulse width. From the above results, we can conclude that the enhanced radiation power is caused by the coherent effect of the undulator radiation due to the electron-beam micropulses having approximately 35-ps pulse width.

The small deviation from the quadratic tendency of the measured power is observed in the relatively high-current region,  $I > 0.3 \text{ A}$ , of Fig. 9. This is caused by the partial saturation of the electron current density in the part of the RPE of Fig. 7, the highest peaks of the electron-beam micropulses cannot increase above the saturation level and the radiation power does not scale as  $N^2$  in this region of the RPE current.

### B. Energy spectrum of the coherent radiation

The total energy spectrum of the coherent radiation,  $dW_i/df$ , at the frequency  $f$  due to  $N$  electrons for a fixed

value of electron-beam pulse width is given by

$$\frac{dW_t}{df} \sim \left[ \frac{dW}{df} \right] NF(f). \quad (11)$$

The inhomogeneous broadening effect in the spectrum was calculated to be negligibly small for the present experimental condition; therefore the deformation of the spectrum by the coherent effect is not caused by the number of electrons having different velocities and trajectories. The numerical calculation by Eq. (11) shows that the spectral width of the coherent radiation spectrum is almost the same as that of the incoherent radiation and that a slight shift of the central frequency towards the lower frequency is also expected due to the effect of the form factor. This value of the central frequency shift is calculated to be 0.3 GHz under the above experimental condition.

Lee *et al.* [15] measured the spontaneous emission spectrum using the same experimental configuration. They used similar experimental parameters and they also observed two-peak wave form of the radiation in the saturated region. Therefore the measured power spectrum is considered to have been that of the coherent radiation. While the spectral width of the measured spectrum was in good agreement with that of the coherent radiation as well as that of the incoherent radiation, the central frequency shift was not observed. This is due to the fact that the fluctuation in radiation power by the random modulation in electron beam did not allow the measurement of the frequency shift of 0.3 GHz.

## VI. CONCLUSION

The coherent effect of undulator radiation has been investigated using a photoelectron beam generated by

fourth harmonics of a *Q*-switched Nd-YAG laser. The Cherenkov radiation emitted by the electron beam through an optical fiber allows one to measure the electron-beam microstructure. The current and temporal structure of the RPE were controlled by changing the incident laser intensity. The unsaturated photoelectron beam was observed to contain a burst of 35-ps micropulses superposed with a weak 8-ns pulse. The intensity of the radiation by the micropulses was more than  $10^3$  times stronger compared to that of the incoherent radiation. The measured power shows quadratic dependence on the electron-beam current. This enhancement and quadratic dependence can be explained by the coherent radiation emitted by the electron-beam micropulses which have a typical bunch length comparable to the radiation wavelength (7.4 mm). The RPE current having a several nanosecond flat top was generated by using the space-charge-limited current density. The radiation power emitted by the RPE having no micropulse was near the noise level of the measurement system, even though the current was much larger than that of the RPE having micropulses. Generation of a high-current and ultrashort electron beam will make it possible to increase the power and to shorten the wavelength of the coherent undulator radiation. High-intensity coherent undulator radiation introduces the possibility for another strong and tunable light source in the millimeter-wavelength range.

## ACKNOWLEDGMENT

We wish to thank Dr. B. C. Lee for valuable help and discussions.

- 
- [1] H. Motz, *J. Appl. Phys.* **22**, 527 (1951).
  - [2] V. N. Baier, V. M. Katkov, and V. M. Strakhovenko, *Zh. Eksp. Teor. Fiz.* **63**, 2121 (1972) [*Sov. Phys. JETP* **36**, 1120 (1973)].
  - [3] A. Hofmann, *Nucl. Instrum. Methods* **152**, 17 (1978).
  - [4] A. Bensussan, J. Bossert, and L. Burnod, *Nucl. Instrum. Methods A* **261**, 343 (1987).
  - [5] A. Amir, I. Boscolo, and L. R. Elias, *Phys. Rev. A* **32**, 2864 (1985).
  - [6] W. A. McMullin and R. C. Davidson, *Phys. Rev. A* **25**, 3130 (1982).
  - [7] W. Becker and J. K. McIver, *J. Appl. Phys.* **58**, 3016 (1985).
  - [8] C. Leubner and P. Torggler, *Opt. Commun.* **48**, 362 (1984).
  - [9] H. A. Haus and M. N. Islam, *J. Appl. Phys.* **54**, 4784 (1983).
  - [10] B. Levush, T. M. Antonsen, and W. M. Manheimer, *J. Appl. Phys.* **60**, 1584 (1986).
  - [11] D. F. Alferov, Yu. A. Bashmakov, and E. G. Bessonov, *Zh. Tekh. Fiz.* **42**, 1921 (1972) [*Sov. Phys. Tech. Phys.* **17**, 1540 (1973)].
  - [12] B. M. Kincaid, *J. Appl. Phys.* **48**, 2684 (1977).
  - [13] H. Motz, W. Thon, and R. N. Whitehurst, *J. Appl. Phys.* **24**, 826 (1953).
  - [14] D. A. G. Deacon, L. R. Elias, J. M. J. Madey, G. J. Ramiyan, H. A. Schwettman, and T. I. Smith, *Phys. Rev. Lett.* **38**, 892 (1977).
  - [15] B. C. Lee, Y. Kawamura, K. Toyoda, M. Kawai, and S. S. Lee, *Appl. Phys. Lett.* **56**, 703 (1990).
  - [16] J. S. Nodvick and D. S. Saxon, *Phys. Rev.* **96**, 180 (1954).
  - [17] T. Nakazato, M. Oyamada, N. Niimura, S. Urasawa, O. Konno, A. Kagaya, R. Kato, T. Kamiyama, Y. Torizuka, T. Nanba, and Y. Kondo, *Phys. Rev. Lett.* **63**, 1245 (1989).
  - [18] J. Ohkuma, S. Okuda, and K. Tsumori, *Phys. Rev. Lett.* **66**, 1967 (1991).
  - [19] Y. U. Jeong *et al.*, *Phys. Rev. Lett.* **68**, 1140 (1992).
  - [20] Y. Kawamura, K. Toyoda, and M. Kawai, *Appl. Phys. Lett.* **45**, 307 (1984).
  - [21] S. W. Downey, L. A. Buita, D. C. Moir, T. J. Ringler, and J. D. Saunders, *Appl. Phys. Lett.* **49**, 911 (1986).